Materials Science & Engineering C 85 (2018) 182–190

Contents lists available at ScienceDirect

Materials Science & Engineering C

journal homepage: www.elsevier.com/locate/msec

Development of porous chitosan/tripolyphosphate scaffolds with tunable uncross-linking primary amine content for bone tissue engineering

Yongxiang Xu, Jianmin Han, Yuan Chai, Shenpo Yuan, Hong Lin*, Xuehui Zhang*

Department of Dental Materials, Peking University School and Hospital of Stomatology, China
National Engineering Laboratory for Digital and Material Technology of Stomatology, China
Beijing Key Laboratory of Digital Stomatology, China

ARTICLE INFO

Keywords:
Chitosan/TPP scaffolds
Uncross-linking primary amine
Ionic-dependent solubility

ABSTRACT

The primary amine along the chitosan backbone plays a key role in biomedical applications. Although chitosan-based porous scaffolds have been widely used in tissue engineering, it remains very challenging to regulate uncross-linking primary amine content (C_N) in scaffolds in order to realize particular mechanical and biological properties. In the present study, chitosan/tripolyphosphate (TPP) scaffolds with controlled C_N (i.e., degree of cross-linking) were prepared based on the ionic-dependent solubility of chitosan together with the freezing process. The effects of the concentration of TPP (C_{TPP}) and NaCl (C_{NaCl}) in the cross-linking solution on C_N were studied by infrared spectroscopy, ninhydrin assays and elemental analysis. The results showed that C_N decreased with increasing C_{TPP} and decreasing C_{NaCl}. C_N affected physicomechanical properties such as swelling behavior and the mechanical strength of the chitosan/TPP scaffolds. The uncross-linking primary amine in scaffolds can be used for chemical and biological modifications. The protein loading of the scaffolds demonstrated that the pH-responsive adsorption and release behavior was influenced by C_N. Cell experiments also illustrated that C_N affected the proliferation of bone marrow mesenchymal stem cells (*BM-MSCs*). All of these results indicate that these porous chitosan/TPP scaffolds containing uncross-linking primary amines are potentially useful for applications in regenerative bone medicine.

1. Introduction

Scaffolds are a platform upon which desired cells proliferate; they play a significant role in tissue engineering by preserving tissue volume, providing temporary mechanical function, and delivering biofactors [1]. A successful scaffold should balance mechanical function with biological properties, including biofactor delivery. Mechanical function has been improved by different cross-linking methods and compositions [2,3]. The delivery of biofactors has been enhanced by changing the junction methods of biofactors; this has included changing physical and chemical junction methods [4]. In addition to improving biocompatibility and biodegradability, research in tissue engineering has focused on improving the mechanical properties and biofactor delivery ability of scaffolds. Polymers, inorganic materials and hybrid materials are widely used for biofactor delivery [5–10].

Chitosan-based scaffolds are widely used in tissue regeneration because chitosan is very similar to naturally occurring glycosaminoglycan and has excellent biocompatibility and biodegradability [11]. Scaffolds made with chitosan alone or a composite have been used to regenerate bone, cartilage, and skin; in addition, scaffolds have been used as drug and protein delivery platforms [12–15]. Three important considerations for a chitosan scaffold include its fabrication, modification and biofactor loading, which are all dependent upon the primary amines of the scaffold. Such structure imparts to chitosan highly valuable physicochemical properties and particular interactions with proteins, cells and living organisms [16]. Bulk chitosan scaffolds have been frequently fabricated via phase separation, lyophilization and neutralization techniques. In addition to these techniques, porogen leaching, microtemplating, and 3D-printing have been used to prepare pore bulk chitosan scaffolds [17]. In all of these methods, the primary amine groups of chitosan were first protonated in dilute acid to dissolve the scaffold, which was then molded into the desired shape. Finally, the protonated amines were neutralized by strong bases, e.g., ammonia and NaOH, to retain the morphology and structure of the bulk scaffold [18]. Hydrogel scaffolds of chitosan were also prepared via physical and chemical cross-linking of the primary amines [19].

Protein adsorption improves the bioactivity of the chitosan scaffold. The primary amines of chitosan can be utilized directly to physically entrap or chemically conjugate growth factors. Peptide/protein-conjugated scaffolds have been prepared by coupling with the primary

* Corresponding authors at: Department of Dental Materials, Peking University School and Hospital of Stomatology, Beijing 100081, China.
E-mail addresses: hong196lin@sina.com (H. Lin), zhangxuehui914@163.com (X. Zhang).

https://doi.org/10.1016/j.msec.2017.12.032
Received 16 June 2017; Received in revised form 23 August 2017; Accepted 28 December 2017
Available online 29 December 2017
0928-4931/

amine groups of chitosan; this further enhanced the functions of the chitosan scaffolds [20–22]. A heparinized chitosan scaffold was fabricated to effectively load biofactors [23,24]. These results suggested that chitosan could be utilized as a base material for scaffold devices as well as delivery vehicles of growth factors for bone healing [25].

It is important to control the uncross-linking primary amine content (C_N) in chitosan scaffolds [26]. The C_N of chitosan/tripolyphosphate (TPP) micro/nano particles can be controlled by the pH of the TPP solution [27]. The advantage of the ionic gelation method using TPP as a crosslinking agent is that it requires only mild conditions that do not damage sensitive proteins or drugs. However, this method is not suitable to prepare bulk scaffolds; when the chitosan solutions are mixed directly with TPP solutions, an instantaneous interaction produces a white precipitate. To date, all of these methods failed to effectively control the C_N of a bulk chitosan scaffold and hindered the modification of the scaffold's properties.

In the present study, bulk chitosan/TPP scaffolds were fabricated with the assistance of NaCl to control the C_N of scaffolds. The effects of preparation conditions on the composition and properties of the scaffolds were studied, and the mechanism was investigated. In addition, the absorption and release of proteins were studied to elucidate the role of uncross-linking primary amine on the pH-responsive delivery of bioactive factors. Furthermore, the effect of the C_N on the cell behavior of rat bone marrow mesenchymal stem cells (BM-MSCs) was also studied.

2. Materials and methods

2.1. Materials

Chitosan ($\overline{M}_\eta$ = 187 kDa, de-acetylation = 89.8%) was purchased from Beijing HWRK Chem Co., Ltd. and purified before use. Acetic acid, phosphate buffer saline (PBS), sodium chloride (NaCl), bovine serum albumin (BSA), dimethyl sulfoxide (DMSO) and other agents were purchased from Sinopharm Chemical Reagent Beijing Co., Ltd. Sodium tripolyphosphate (TPP), ninhydrin and glycine were purchased from Sigma-Aldrich Co. A BCA assay kit was obtained from Thermo Scientific. All chemicals were analytical grade and used without further purification. Rat bone marrow mesenchymal stem cells (BM-MSCs) were purchased from Cyagen Bioscience, Guangzhou, China.

2.2. Preparation of chitosan scaffolds

Chitosan was dispersed in deionized water and a stoichiometrically equivalent amount of acetic acid was added. After complete dissolution, the pH of the solution (20 mg/ml) was adjusted to 5.0 by 0.5 M NaOH and it was left to stand for 24 h without stirring for degassing at 4 °C. The solution was injected into a mold and frozen at − 20 °C for 24 h. The frozen chitosan was immersed in a saturated NaCl solution at − 20 °C for 48 h and then stored at 23 °C. After that, the sample was immersed in a crosslinking solution with different concentrations of TPP (C_{TPP}) and NaCl (C_{NaCl}) at pH = 5.0 for 24 h to prepare chitosan scaffolds. Different C_{NaCl} values (0.05/0.5/1.5/3/4.5/6 M) with the same C_{TPP} (1% [w/w]) were studied, as were different C_{TPP} values (0.25/0.5/2.0/4.0/6.0% ([w/w]) with the same C_{NaCl} (3 M). Finally, all the samples were washed thoroughly with de-ionized water to remove residual TPP and NaCl.

2.3. Composition and structure

2.3.1. Infrared spectroscopy

The compositions of scaffolds were first characterized by an attenuated total reflectance-Fourier transform infrared (*ATR-FTIR*) spectrometer (Nicolet iN10 Spectrometer, MA, USA). The spectra in the range of 600–4000 cm^{-1} were collected in 32 scans at 4 cm^{-1} resolution.

2.3.2. Ninhydrin assays

The C_N of scaffolds was determined by ninhydrin assays [19]. The test samples were lyophilized for 24 h and weighed. Subsequently, the test samples were heated with 2% (w/v) ninhydrin solution for 20 min at 100 °C. The C_N in the test samples were determined by the optical absorbance of the solution at 570 nm recorded with a microplate reader (SpectraMax Plus 384, Molecular Devices LLC, USA) using glycine as the standard. Each determination was performed in triplicate. The C_N was calculated as follows:

$$C_N\ (\%) = W_{N-1}/W_{N-0} \times 100\%$$

The amount of uncross-linking primary amine was represented as "W_{N-1}" for the cross-linked samples and "W_{N-0}" for the original chitosan sample (non-cross-linked).

2.3.3. Morphology and elemental composition

The liquid-nitrogen fracture surfaces of the scaffolds were characterized using a scanning electron microscope (SEM, EVO 18, Zeiss, Oberkochen, Germany) after lyophilization. The elemental analysis was performed using an attachment EDS (INCA X-Act; Oxford Instruments PLC, Abingdon, UK) of SEM. The phosphorus content (C_P), which represents the content of cross-linking primary amine in scaffolds, was calculated as follows:

$$C_P\ (\%) = W_P/(W_C + W_N + W_O + W_P) \times 100\%$$

Herein, the terms "W_C", "W_N", "W_O" and "W_P", represent the weight fractions of C, N, O and P elements, respectively.

2.4. Physico-mechanical properties

2.4.1. Swelling behavior

The water sorption capacity of chitosan scaffolds was determined by swelling the lyophilized scaffold in de-ionized water for 24 h. The images of scaffolds were captured by a digital camera (EOS 5D Mark II, Canon, Tokyo, Japan). An electronic balance was used to determine the weight of lyophilized scaffolds (W_0) and swelling scaffolds (W_1). The percent swelling ratio (R_s) of scaffolds at equilibrium was calculated according to the following equation:

$$R_s\ (\%) = (W_1 - W_0)/W_0 \times 100\%$$

2.4.2. Mechanical properties

The Young's modulus (E) of the chitosan scaffolds was determined by compression testing at a rate of 5.0 mm/min at a temperature of 23 °C using a universal material testing machine (model 5543A, Instron, Norwood, MA, USA). Rheological measurements were carried out at 37 °C with a rheometer (Physica MCR301, Anton Paar, Graz, Austria) operating with a plate-plate geometry (diameter: 25 mm). Strain amplitude values were verified to ensure that all measurements were performed within the linear viscoelastic range to obtain storage modulus (G') and loss modulus (G'') independent of strain amplitude. Samples with a thickness of 3.0 mm were introduced between the plates. All experiments were repeated three times.

2.5. Cytotoxicity assays

The cytotoxicity of the scaffolds was evaluated using extracts and L929 fibroblast cells (ATCC, Manassas, VA, USA) following ISO 10993-5:2009 standards. The test scaffold extract was prepared with 0.5, 1.0, and 1.5 mg of chitosan in 1 mL of minimum essential medium at 37°C for 24 h. The blank culture medium and 10% DMSO were used as negative and positive controls, respectively. The optical intensity was measured at a wavelength of 570 nm using the microplate reader. The cytotoxicity of the hydrogel was expressed as % cell viability, which was calculated from the ratio between the number of cells treated with the polymer solutions and that of non-treated cells (control).

2.6. Protein adsorption and release

2.6.1. BSA adsorption

Adsorbing growth factors into dehydrated hydrophilic polymer networks has been the most commonly used approach to incorporate growth factors into scaffolds in the clinic. For the loading of bioactivity factors, BSA was used as the model protein. Each lyophilized scaffold of 5 mg was immersed in 1 mL PBS solution (pH = 3.0/6.0/7.4) containing BSA (C_0 = 0.5 mg/ml) at room temperature to access the protein's adsorption behavior. After 24 h with shaking, the supernatant was collected and its concentration (C_1) was assayed with a BCA assay kit on the microplate reader at 570 nm. Three replicate samples were tested for all experiments. BSA-loading efficiency (R_e) was calculated using the weight of BSA trapped by the scaffold as a percentage of the total protein added, as follows:

$$R_e\,(\%) = (C_0 - C_1)/C_1 \times 100\%$$

2.6.2. BSA release

The BSA-loading scaffolds formed from the cross-linking solution (3 M NaCl + 1% (w/w) TPP) was further used to examine the release behavior. Each sample with 5 mg was immersed in 5 mL PBS solution (pH = 3.0/6.0/7.4) while shaking. At predetermined time points (0.5, 1.0, 2.0, 4.0, 8.0, 12.0, 16.0 h and 1, 2, 3, 4, 5, 6, 7 days), 0.5 ml supernatant was sampled and replaced with an equal volume of fresh PBS. The BSA concentration was also assayed with a BCA assay kit, and the cumulative amount of BSA released from the scaffold was calculated from the standard curve of BSA. Three replicate samples were tested for all experiments.

2.7. Proliferation and adhesion of immobilized cells

Rat BM-MSCs were cultured in Dulbecco's modified eagle medium supplemented with 10% fetal bovine serum and 100 IU/mL penicillin-streptomycin. The medium was changed every 2 days. At 80–90% confluence, BM-MSCs were detached with 0.25% trypsin/ethylenediaminetetraacetic acid. The cells from 3 to 5 passages were used in the following studies.

BM-MSCs (1.2×10^5 cells/well) were seeded onto an experimental scaffold in 48-well plates and incubated at 37 °C in a humidified atmosphere with 5% CO_2. After 24 h of culture, attached cells were fixed with 4% paraformaldehyde, incubated with rhodamine-phalloidin (100 nmol/L) for 1 h and then stained with 4′, 6-diamidino-2-phenylindole (DAPI) for 1 min based on the manufacturer's directions. Fluorescence images of stained constructs were obtained using a confocal laser scanning microscope (Carl Zeiss Microimaging, Oberkochen, Germany).

3. Results and discussion

3.1. Fabricating process and mechanism

The freezing process and ionic strength-dependent solubility of chitosan were combined to fabricate bulk chitosan/TPP scaffold. As illustrated in Scheme 1, the fabricated mechanism is as follows. First, the primary amines (pKa = 6.3) of chitosan are protonated in acetic acid solution ($-NH_2$ to $-NH_3^+$), which causes electrostatic repulsion between the polymer chains, rendering the corresponding chitosan-acetate soluble [28]. Second, ice crystals form in the chitosan solution upon freezing and are phase-separated from the chitosan acetate salt [29]. Third, the ice inside the frozen samples is gradually replaced by the saturated NaCl solution at − 20 °C. The high ionic strength (Cl^-) electronically screens the $-NH_3^+$ and induces screening of the electrostatic repulsion between the polymer chains and prevents its dissolution; therefore, the scaffold retains the interconnected pore network and original outside morphology at 23 °C [30]. Finally, in the cross-linking solution that includes both NaCl and TPP, Cl^- in the sample diffuses out and the TPP diffuses into the cross-linking solution because of the concentration gradient. Some of the $-NH_3^+$ groups that are no longer electronically screened by Cl^- are cross-linked by TPP and scaffolds form with controlled uncross-linking primary amine content [27].

3.2. Compositions

ATR-FTIR spectra were used to qualitatively characterize the composition of the chitosan scaffolds, as shown in Fig. 1. In the IR spectra of cross-linked chitosan, the peak at 1544 cm^{-1} disappears partly and two new peaks at 1620 cm^{-1} and 1525 cm^{-1} appear. A characteristic band at 1544 cm^{-1} is attributed to the primary amine groups of chitosan. The disappearance of the band was attributed to the linkage between the phosphoric and ammonium ions [31]. The increase in the intensity of the peaks at 1620 cm^{-1} and 1525 cm^{-1} indicates an increase of bound TPP ions [32,33]. This result was attributed to the increase of interchain linkages of $-NH_3^+$ groups in chitosan by TPP ions. It demonstrated that the ionic reaction of chitosan/TPP scaffolds was significantly influenced by the composition of the cross-linking solution, and the ionic cross-linking degree increased with either increasing C_{TPP} or decreasing C_{NaCl}.

Ninhydrin assays were used to determine the extent of the various types of cross-linking reactions by quantifying the C_N in the test sample, expressed in terms of the glycine concentration [34,35]. Fig. 2 shows the C_N of chitosan/TPP scaffolds made under different fabrication conditions (C_{TPP} and C_{NaCl}). The data reveal that the least amount ($C_N \approx 17\%$) of uncross-linking primary amine corresponded to the scaffold that was ionically cross-linked with the most C_{NaCl}, probably because of the great extent of ionic interaction. The addition of NaCl drastically increases the quantity of uncross-linking primary amine and tends to hinder ionic cross-linking, suggesting the effect of electronical screening of NH_3^+ by Cl^-. The same results were observed with increasing C_{TPP} at the same C_{NaCl}. This observation is in accord with the results obtained from IR analyses.

The elemental compositions of scaffolds were used to determine the quantity of TPP that reacted with the primary amine groups of chitosan [36]. Fig. 3 indicates that the C_P in scaffolds increased with either increasing C_{TPP} or decreasing C_{NaCl}. In addition to intermolecular and intramolecular linkages between linear chitosan chains, a single linkage formed between a chitosan chain and TPP. Only the intermolecular linkages were attributed to the cross-linking degree of the chitosan/TPP scaffold. As a result, the high phosphorus content was not necessarily equal to a high degree of cross-linking. IR spectra, ninhydrin assays and physico-mechanical properties were evaluated to determine the cross-linking of chitosan/TPP scaffolds.

3.3. Microstructure

Fig. 4 presents SEM micrographs of the internal structure of chitosan/TPP scaffolds prepared under different conditions. An open network structure is observed in all the samples that appears to be highly porous with interconnected macrodomains [37]. These pores possessed similar shapes with a polygonal cross section. The pore sizes of scaffolds ranged from 50 to 150 μm and increased with either increasing C_{NaCl} or decreasing C_{TPP}.

3.4. Swelling behavior

To ascertain the potential use of ionically cross-linked hydrogels as biomaterials for biomedical applications, their swelling capacities must be evaluated. Swelling is primarily influenced by ionic interactions between chitosan chains, which depends in turn on the degree of cross-linking [38]. In de-ionized water, the ionic-crosslinked chain of a chitosan-TPP complex didn't dissociate; therefore, the swelling of the

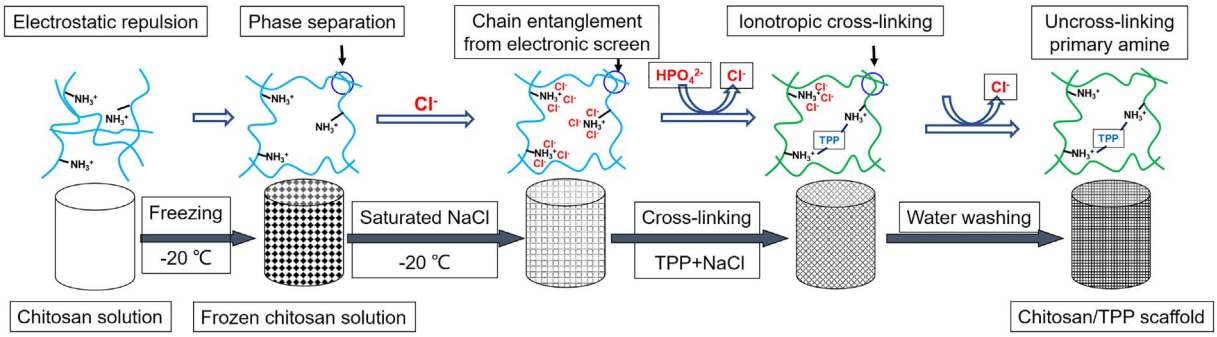

Scheme 1. Schematic illustration of the process and mechanism for fabrication of bulk chitosan/TPP scaffolds with uncross-linking primary amine.

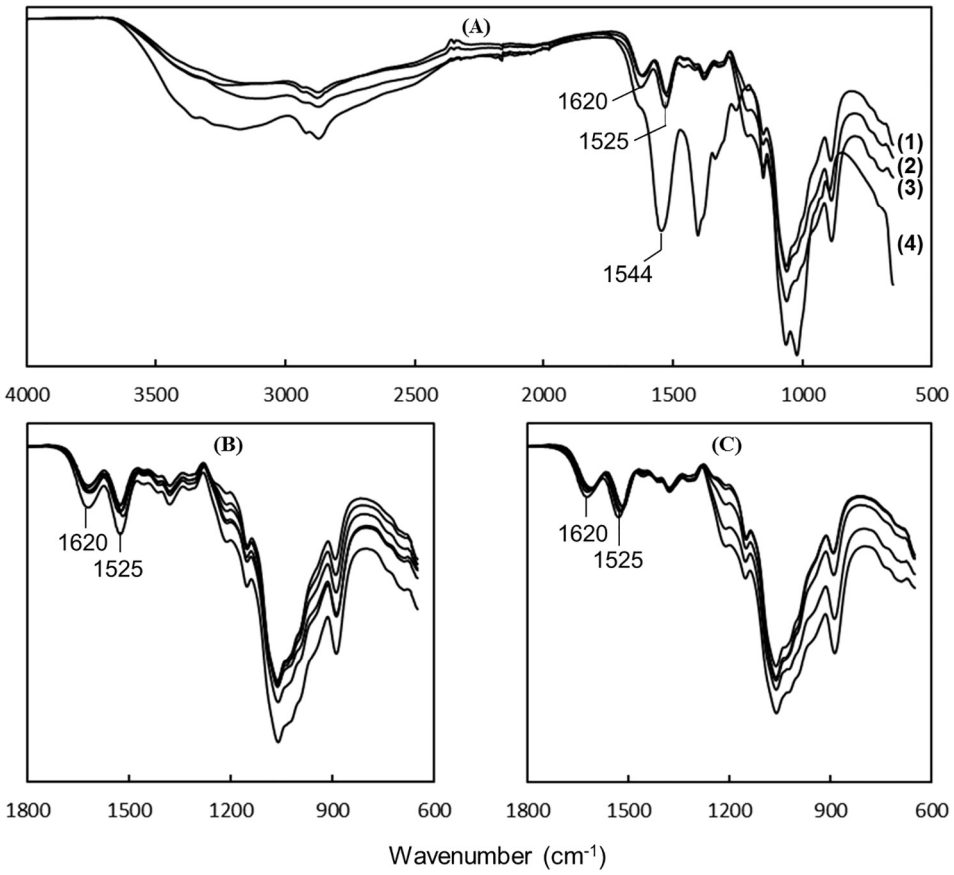

Fig. 1. ATR-FTIR spectra of chitosan/TPP scaffolds. (A) The reaction of chitosan and TPP: (1) 0.5 M NaCl + 1% (w/w) TPP, (2) 3 M NaCl + 1% (w/w) TPP, (3) 3 M NaCl + 4% (w/w) TPP, (4) chitosan without TPP (control). Section of spectra showing an enlargement of a section in the region 650–1800 cm^{-1}: (B) From top to bottom, 0.05/0.5/1.5/3/4.5/6 M NaCl + 1% (w/w) TPP and (C) from top to bottom, 3 M NaCl + 0.25/0.5/2/4/6% (w/w) TPP.

scaffold was attributable to the hydration or ionization of uncross-linking primary amines in chitosan. Chitosan scaffolds swell easily in aqueous solution due to the high density of protonated amine groups that have a strong affinity for water molecules. As illustrated in Fig. 5, the lyophilized samples are the white scaffolds and semi-transparent samples are observed after swelling in water. Furthermore, the

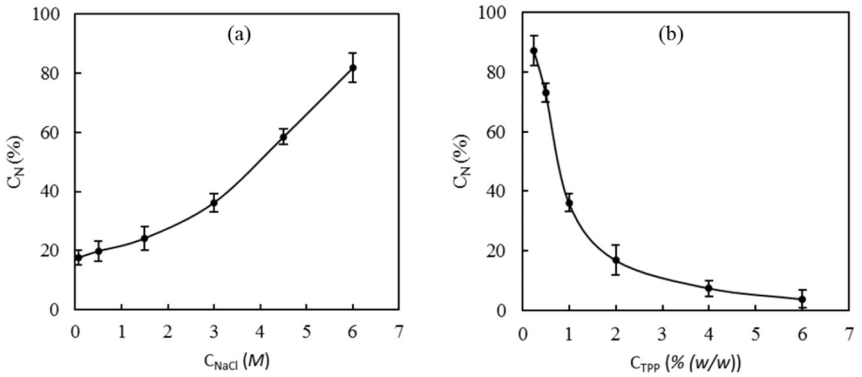

Fig. 2. The uncross-linking primary amine content (C_N) of chitosan/TPP scaffolds with different fabrication conditions: (a) Effect of C_{NaCl} on the scaffolds prepared with 1% (w/w) TPP; (b) effect of C_{TPP} on the scaffolds prepared with 3 M NaCl.

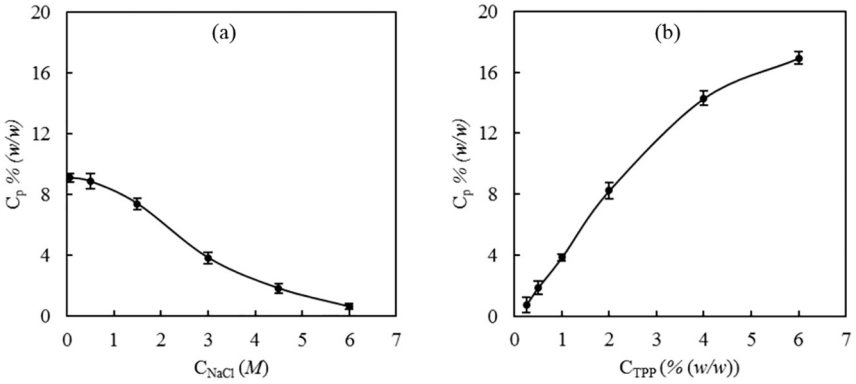

Fig. 3. The phosphorus content (C_P) of chitosan/TPP scaffolds with different fabrication conditions: (a) Effect of C_{NaCl} on the scaffolds prepared with 1% (w/w) TPP; (b) effect of C_{TPP} on the scaffolds prepared with 3 M NaCl.

transparent intensity and the size of the samples increased with either decreasing C_{TPP} or increasing C_{NaCl} because of the change of C_N and the densities of the samples. This observation is compatible with the data of R_s. That is, R_s increased with either decreasing C_{TPP} or increasing C_{NaCl}. Higher R_s values, larger size and higher C_N. This contradicts the results given in Figs. 1 & 2 that revealed that the sample contained different C_N.

3.5. Mechanical properties

Appropriate mechanical properties are required for scaffolds that are used for tissue engineering and regenerative medicine. The mechanical properties (E, G' and G'') of scaffolds are illustrated in Fig. 6. As C_{NaCl} increased from 0 to 6 M, E decreased from 38 kPa to 2.4 kPa. As C_{TPP} increased from 0.25% (w/w) to 6% (w/w), E increased from 0.85 kPa to 12.6 kPa. The C_{NaCl} and C_{TPP} have the same effects on the rheological properties (G' & G'') as E. The increasing mechanical properties indicated an increasing degree of cross-linking (decreasing C_N), which contradicts the above results about the composition of the scaffolds.

3.6. Mechanism analysis

The presence of non-gelling ions (i.e. Na^+ and Cl^-) played a key role in the crosslinking process between chitosan and TPP. At pH = 5.0, TPP dissociates to form $H_3P_3O_{10}{}^{2-}$ and $2H^+$. Typically, $H_3P_3O_{10}{}^{2-}$ anions quickly cross-link the protonated amine group of chitosan, leading to the formation of nanoparticles or aggregates as soon as TPP solution is added to chitosan solutions [38]. However, in the present study, the presence of large amounts of Na^+ and Cl^- partly prevented the gelation process by screening the strong electrostatic interactions between the polymer and crosslinker. When the C_{NaCl} in the crosslinking solution was lower than the saturated concentration, the Na^+ and Cl^- in the chitosan sample diffused into the crosslinking solution because of the concentration gradient. Simultaneously, the $H_3P_3O_{10}{}^{2-}$ diffused into the chitosan sample. Then, the $-NH_3{}^+$ that had not been

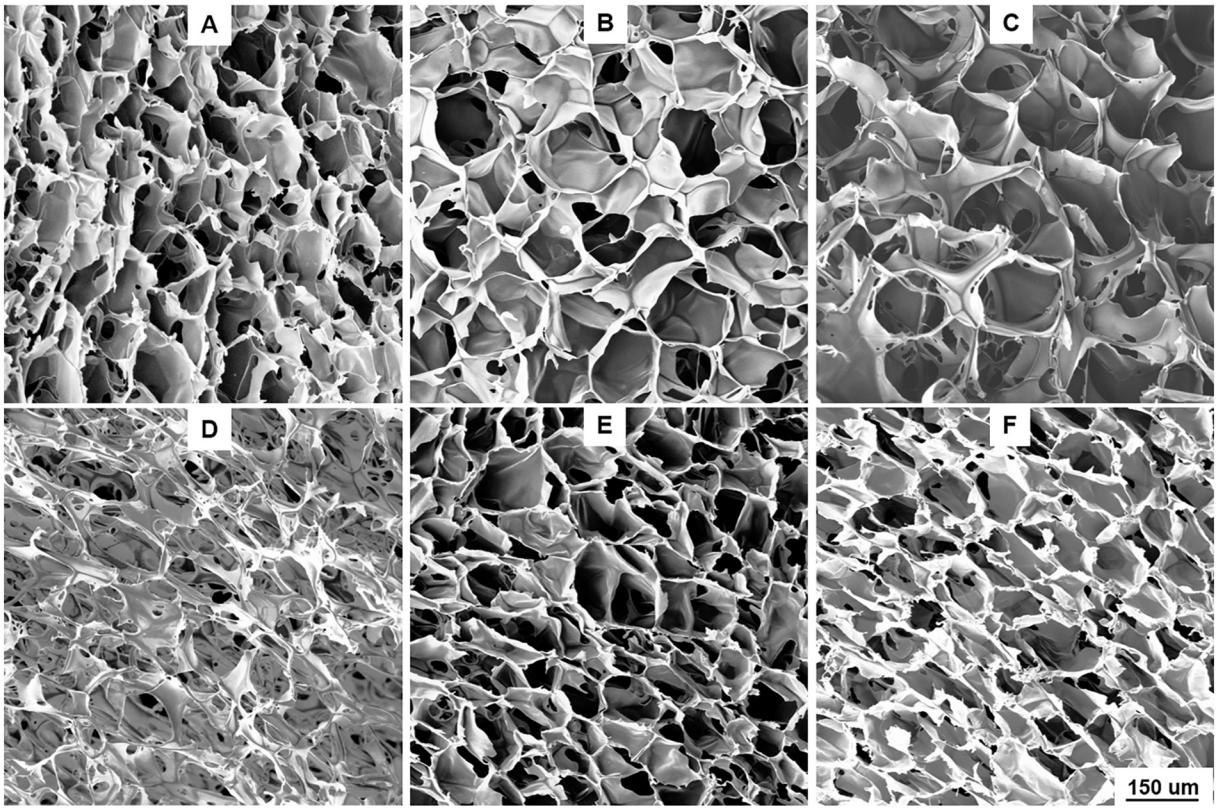

Fig. 4. SEM images (× 200) of scaffolds prepared in different cross-linking solutions: (A) 1% (w/w) TPP, (B) 3 M NaCl + 1% (w/w) TPP, (C) 6 M NaCl + 1 (w/w) % TPP, (D) 3 M NaCl + 0.25 (w/w) % TPP, (E) 3 M NaCl + 2% (w/w) TPP, (F) 3 M NaCl + 6 (w/w) % TPP.

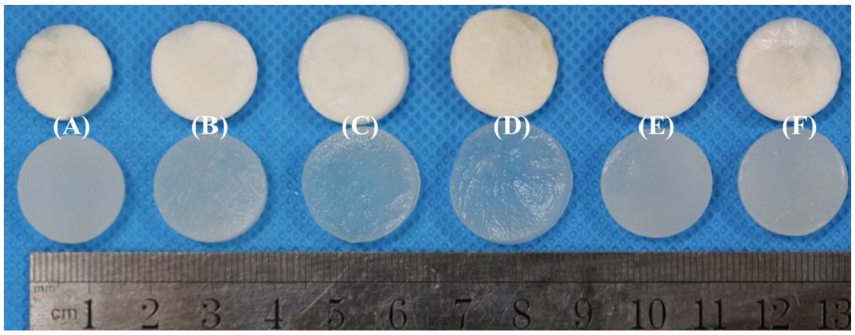

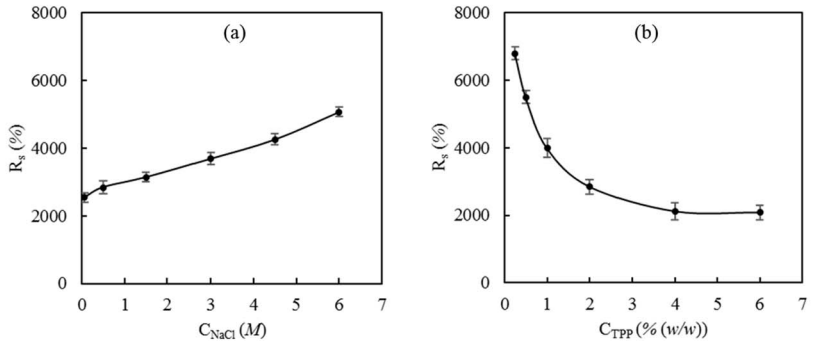

Fig. 5. Swelling behavior of chitosan scaffolds. Top: Morphologies of chitosan scaffolds before and after swelling: (A) 1% (w/w) TPP, (B) 3 M NaCl + 1% (w/w) TPP, (C) 6 M NaCl + 1 (w/w) % TPP, (D) 3 M NaCl + 0.25 (w/w) % TPP, (E) 3 M NaCl + 2% (w/w) TPP, (F) 3 M NaCl + 6 (w/w) % TPP. Bottom: The effect of preparation conditions on the swelling ratio (R_s) of scaffolds: (a) Effect of C_{NaCl} on the scaffolds prepared with 1% (w/w) TPP; (b) effect of C_{TPP} on the scaffolds prepared with 3 M NaCl.

screened by Cl^- was ionically-crosslinked by $H_3P_3O_{10}{}^{2-}$. The complex that formed between $-NH_3{}^+$ and $H_3P_3O_{10}{}^{2-}$ was irreversible and more stable than the complex that formed between $-NH_3{}^+$ and Cl^-. However, the quantity of Cl^- was higher than that of $H_3P_3O_{10}{}^{2-}$ and some $-NH_3{}^+$ was always screened by Cl^-. As a result, the crosslinking between $-NH_3{}^+$ and $H_3P_3O_{10}{}^{2-}$ varied based upon the C_{TPP} and C_{NaCl} in the cross-linking solution. The degree of cross-linking increased with increasing C_{TPP} and decreasing C_{NaCl}.

3.7. In vitro cytotoxicity

The cytotoxicity of the chitosan hydrogel was determined using a 3-(4,5)-dimethylthiahiazo(-z-y1)-3,5-di-phenytetrazoliumromide (MTT) assay. As illustrated in Fig. 7, all the samples demonstrated cytocompatibility for fibroblast cells. These findings are consistent with previous research results [39,40].

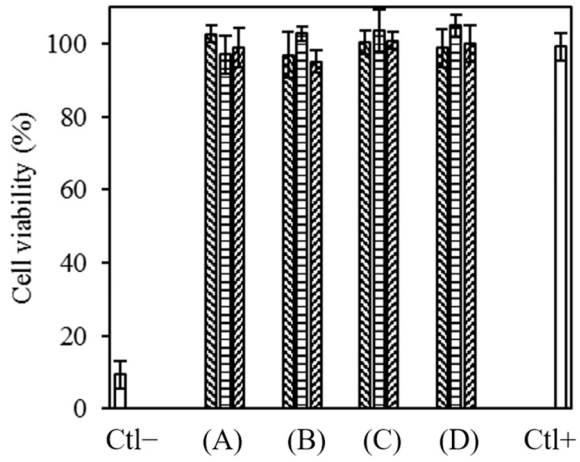

Fig. 7. Viability of L929 fibroblasts exposed to extracts during incubation with various scaffolds at different concentrations (0.5, 1.0 and 1.5 mg/ml). (A) 0.05 M NaCl + 1% (w/w) TPP; (B) 6 M NaCl + 1% (w/w) TPP; (C) 3 M NaCl + 0.25% (w/w) TPP; (D) 3 M NaCl + 6% (w/w) TPP. Ctl −, 10% DMSO; Ctl +, medium culture.

3.8. Protein adsorption and release

Protein adsorption is known to influence cell adhesion by adsorption of key adhesion molecules like fibronectin or vitronectin. The protein loading in a scaffold depends upon the physical and chemical properties of the scaffold as well as the structural features of the different proteins [41]. In this research, BSA was used as the model protein and its isoelectric point is 4.7. In solutions with pH < 4.7, the net charge of BSA is expected to be positive (BSA^+), whereas the net charge of BSA is expected to be negative (BSA^-) for pH > 4.7 [42].

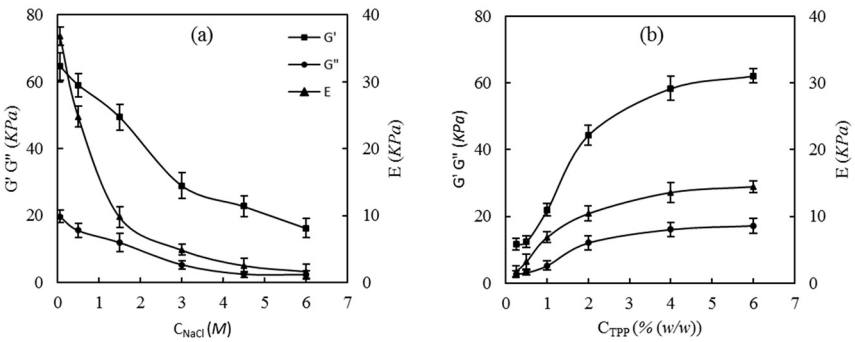

Fig. 6. The mechanical properties, compressive elastic modulus (E), storage modulus (G') and loss modulus (G''), of chitosan/TPP scaffolds prepared in different fabrication conditions: (a) Effect of C_{NaCl} on the scaffolds prepared with 1% (w/w) TPP; (b) effect of C_{TPP} on the scaffolds prepared with 3 M NaCl.

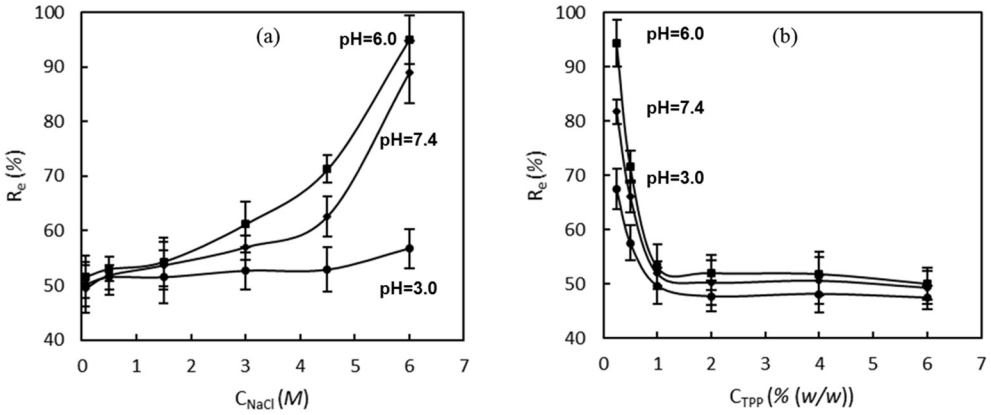

Fig. 8. BSA-loading efficiency (R_e) in BSA solution at different pH values (3.0/6.0/7.4) of chitosan/TPP scaffolds, with different fabrication conditions: (a) Effect of C_{NaCl} on the scaffolds prepared with 1% (w/w) TPP; (b) effect of C_{TPP} on the scaffolds prepared with 3 M NaCl.

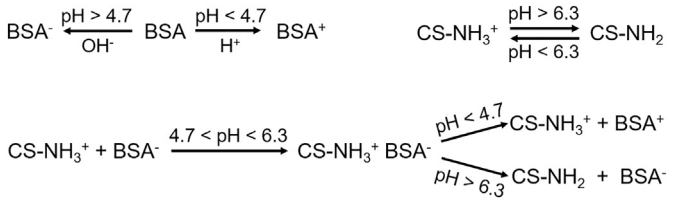

Fig. 9. The mechanism of BSA adsorption and release in chitosan/TPP scaffolds with uncross-linking primary amine.

The R_e of chitosan scaffolds was affected by the fabricating conditions and was pH-responsive. BSA was dissolved in PBS at different pH's (3.0, 6.0 and 7.4) to maintain the pH of the solution in the adsorption process. Fig. 8 shows that R_e = 45–95% and was significantly affected by the properties of the scaffolds and the pH of BSA solution. The R_e increased with increasing C_{NaCl} and decreasing C_{TPP}. Furthermore, the R_e was higher in the BSA solution with pH = 6.0/7.4 than pH = 3.0.

Fig. 9 illustrates the mechanism of BSA adsorption and release in chitosan/TPP scaffolds. When the lyophilized scaffolds were immersed into the BSA solution while stirring, BSA diffused into the scaffold through the porosity created by the concentration gradients. BSA interacted with the scaffolds via a combination of long-range (e.g., electrostatic) and short-range noncovalent (van der Waals, hydrophobic, hydrogen bonding) interactions [43]. At pH = 3.0 (< 4.7), BSA^+ has an electrostatic repulsion with the $-NH_3^+$ groups of the scaffolds. At pH = 6.0 (> 4.7 and < 6.3), BSA^- has an electrostatic attraction with the $-NH_3^+$ groups of the scaffolds. At a pH value of 7.4 (> 4.7 and > 6.3), the $-NH_3^+$ groups of the scaffolds were neutralized to $-NH_2$ by both OH^- and BSA^-. Different fabrication conditions (C_{NaCl} and C_{TPP}) resulted in different concentrations of $-NH_3^+$ (cross-linking degree) and different R_e values. The R_e was highest (electrostatic attraction) at pH = 6.0, followed by the R_e at pH = 7.4 (part electrostatic attraction). The R_e was lowest at pH = 3.0 (electrostatic repulsion). Furthermore, the minimum R_e was 46% which indicated that there was another type of short-range adsorption, beside the electrostatic interaction.

The pharmacokinetics of growth factor delivery has been a critical regulator of scaffolds' clinical success. As shown in Fig. 10, BSA release in PBS with different pH values (3.0/6.0/7.4) from chitosan scaffolds proceeded in two distinct phases: 1) an initial burst release (1 day) which was followed by, 2) a period of sustained release (1–7 days). The initial burst phase of protein release could be attributed to protein that was electrostatically repulsed from the scaffold and surface-bound protein that rapidly diffused away. After that, the complexes formed between BSA^- and $-NH_3^+$ dissociated and BSA was released continuously.

A dissolution-diffusion model with pH-responsive release behavior could be used to describe the BSA release from scaffolds [44]. For the BSA-scaffold that formed at pH = 3.0, the releasing rate of BSA in PBS was (pH = 3.0) > (pH = 6.0) > (pH = 7.4). When the scaffolds were immersed in PBS at pH = 3.0, all of the BSA^+ that had been adsorbed as a result of the concentration gradient would then be released because of the concentration gradient; the electrostatic repulsion would accelerate this process. When in PBS with pH = 6.0/7.4, some of the BSA^+ changed to BSA^-, which was then electrostatically attracted to the $-NH_3^+$ groups of the scaffolds; this decelerated the releasing rate. More BSA^- formed at pH = 7.4 than at pH = 6.0, resulting in a diminished release of BSA. For the BSA-scaffold that formed at pH = 6.0, the releasing rate of BSA in PBS was (pH = 3.0) > (pH = 7.4) > (pH = 6.0). In PBS with pH = 3.0, the complexes of $-NH_3^+ \cdot BSA^-$ dissociated and BSA^+ was released by concentration gradient and electrostatic repulsion. Some of the $-NH_3^+$ groups were neutralized by OH^- and BSA^- at pH = 7.4; this reduced the electrostatic repulsion. Only the BSA that was not adsorbed by electrostatic

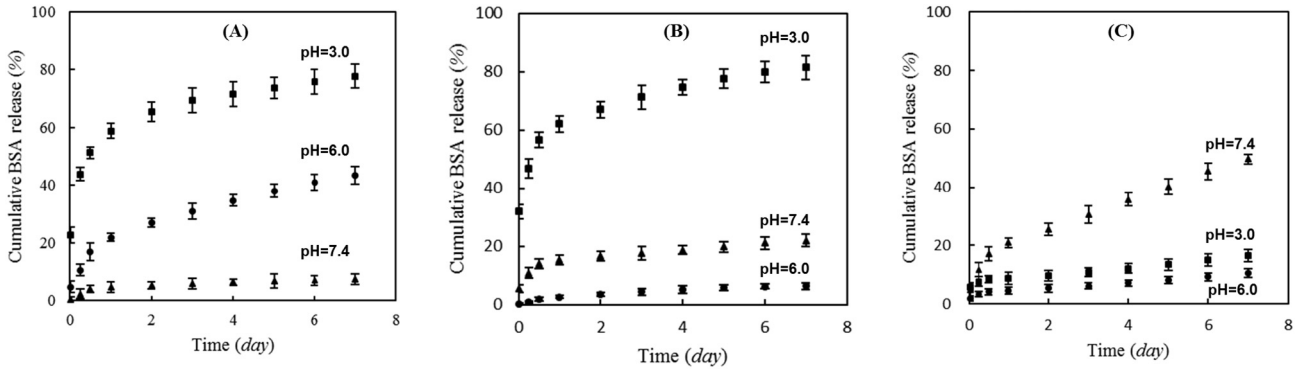

Fig. 10. Cumulative BSA release (%) in PBS with different pH values (3.0/6.0/7.4) from the BSA-loaded scaffolds (3 M NaCl + 1% (w/w) TPP) which adsorbed BSA from different BSA solutions: (A) pH = 3.0, (B) pH = 6.0, (C) pH = 7.4.

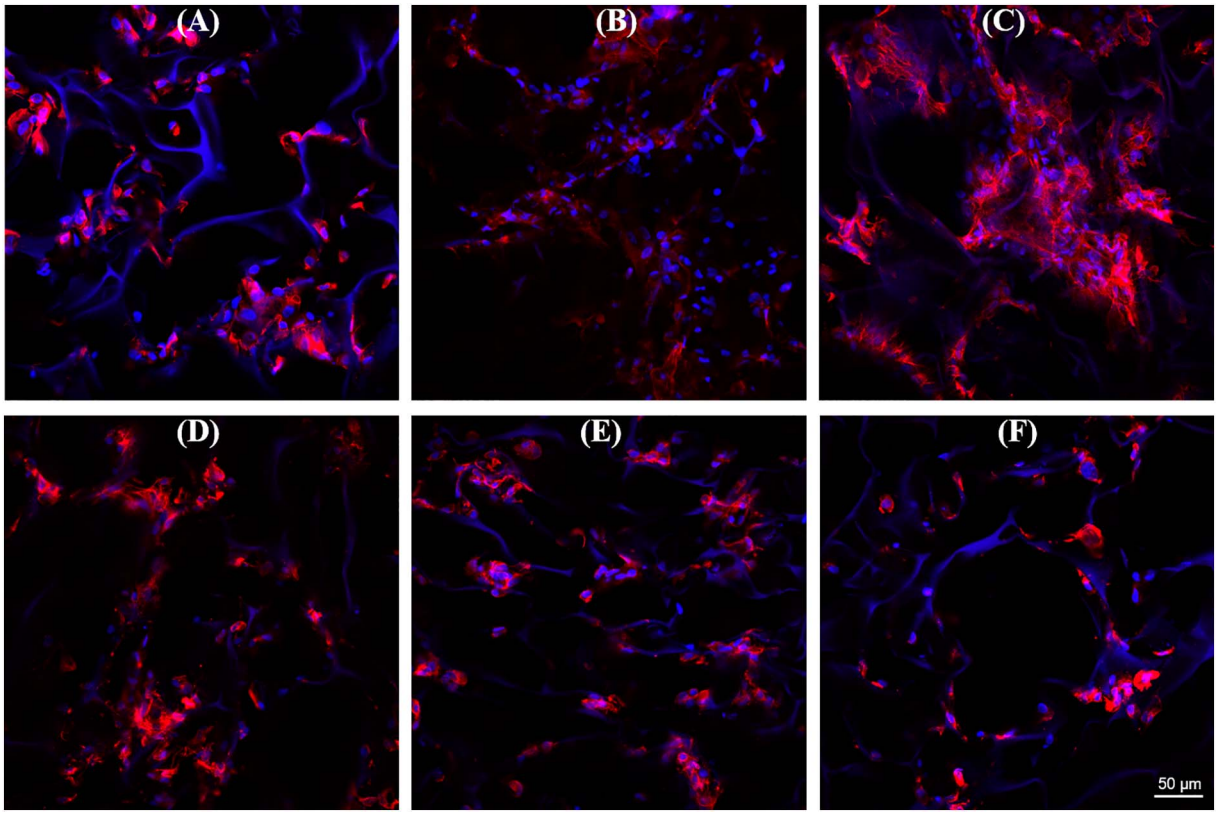

Fig. 11. Confocal micrographs of rat *BM-MSCs* on chitosan scaffolds formed in different conditions: (A) 1% (w/w) TPP, (B) 3 M NaCl + 1% (w/w) TPP, (C) 6 M NaCl + 1 (w/w) % TPP, (D) 3 M NaCl + 0.25 (w/w) % TPP, (E) 3 M NaCl + 2% (w/w) TPP, (F) 3 M NaCl + 6 (w/w) % TPP. Actin network is shown in red with rhodamine-phalloidin and nuclei are shown in blue with DAPI after 24 h of culture. The chitosan fibres are also shown in green, due to the autofluorescence signal of chitosan. (For interpretation of the references to color in this figure legend, the reader is referred to the web version of this article.)

attraction was released into PBS at pH = 6.0. For the BSA-scaffold that formed at pH = 7.4, the releasing rate of BSA in PBS was (pH = 7.4) > (pH = 3.0) > (pH = 6.0); this trend also resulted from the change in charges in the environment. In summary, BSA joins chitosan in chitosan scaffolds by electrostatic attraction and by other interactions. When the BSA-loading scaffolds at 1 pH value were immersed in the releasing medium with another pH value, the BSA would change to BSA^+ or BSA^- and NH_2 would change to NH_3^+. Further electrostatic attractions or repulsions would form in the releasing medium which accelerated or decelerated the releasing rate of BSA.

3.9. Cell behavior of rat BM-MSCs

The adhesion of BM-MSCs onto the scaffolds was assessed by confocal microscopy (Fig. 11). The images indicated that cells could adhere to the fibres of the chitosan scaffolds after 24 h of culture. The results showed that the number of BM-MSCs increased with either increasing C_{NaCl} or decreasing C_{TPP}. As shown in Fig. 4, the pore sizes of the scaffolds increased with either increasing C_{NaCl} or decreasing C_{TPP}. Normally, the number of cells increased with decreasing pore size, increasing the density of the chitosan fibres. The opposite tendency observed in the present study indicates that the C_N of the chitosan/TPP scaffold played a significant role for the adhesion and proliferation of BM-MSCs. A higher C_N resulted in a higher number of cells.

4. Conclusions

This work demonstrates that it is possible to prepare bulk chitosan/TPP scaffolds with different uncross-linking primary amine content. For this, the ionic strength-dependent solubility of chitosan was used to control the extent of reaction between chitosan and TPP in the presence of NaCl. The un-crosslinking primary amine in the scaffolds affected the mechanical properties, protein adsorption and cell behavior. This study provided an innovative and well-suited strategy for controlling the uncross-linking primary amine content in chitosan/TPP scaffolds for bone regenerative therapies; this study also provided a foundation for further modifications of scaffolds, pH-responsive adsorption and the release of drugs or proteins from the scaffolds.

Acknowledgements

This work was supported by the National Natural Science Foundation of China [grant numbers 81200814, 51502006], the National High-tech R&D Program of China [grant number 2015AA033601] and the Young Elite Scientist Sponsorship Program of China Association for Science and Technology (CAST) [grant number 2016QNRC001].

References

[1] S.J. Hollister, Porous scaffold design for tissue engineering, Nat. Mater. 4 (2006) 518–524.
[2] F.J. O'Brien, Biomaterials & scaffolds for tissue engineering, Mater. Today 14 (2011) 88–95.
[3] S.F. Badylak, D.O. Freytes, T.W. Gilbert, Extracellular matrix as a biological scaffold material: structure and function, Acta Biomater. 5 (2009) 1–13.
[4] M.J. Whitaker, R.A. Quirk, S.M. Howdle, K.M. Shakesheff, Growth factor release from tissue engineering scaffolds, J. Pharm. Pharmacol. 53 (2001) 1427–1437.
[5] E. Ye, M.D. Regulacio, S.Y. Zhang, X.J. Loh, M.Y. Han, Anisotropically branched metal nanostructures, Chem. Soc. Rev. 44 (2015) 6001–6017.
[6] E. Ellis, K. Zhang, Q. Lin, E. Ye, A. Poma, G. Battaglia, J.L. Xian, T.C. Lee, Biocompatible pH-responsive nanoparticles with a core-anchored multilayer shell of triblock copolymers for enhanced cancer therapy, J. Mater. Chem. B 5 (2017) 4421–4425.
[7] C.P. Teng, T. Zhou, E. Ye, S. Liu, L.D. Koh, M. Low, X.J. Loh, K.Y. Win, L. Zhang, M.Y. Han, Effective targeted photothermal ablation of multidrug resistant bacteria

and their biofilms with NIR-absorbing gold nanocrosses, Adv. Healthc. Mater. 5 (2016) 2122–2130.
[8] R. Lakshminarayanan, X.J. Loh, S. Gayathri, S. Sindhu, Y. Banerjee, R.M. Kini, S. Valiyaveettil, Formation of transient amorphous calcium carbonate precursor in quail eggshell mineralization: an in vitro study, Biomacromolecules 7 (2006) 3202–3209.
[9] R. Tan, H. Zhu, C. Cao, O. Chen, Multi-component superstructures self-assembled from nanocrystal building blocks, Nano 8 (2016) 9944–9961.
[10] E. Ye, X.J. Loh, Polymeric hydrogels and nanoparticles: a merging and emerging field, Aust. J. Chem. 66 (2013) 997–1007.
[11] J.L. Drury, D.J. Mooney, Hydrogels for tissue engineering: scaffold design variables and applications, Biomaterials 24 (2003) 4337–4351.
[12] S.P. Miguel, M.P. Ribeiro, H. Brancal, P. Coutinho, I.J. Correia, Thermoresponsive chitosan-agarose hydrogel for skin regeneration, Carbohydr. Polym. 111 (2014) 366–373.
[13] R. Jin, L.S. Moreira Teixeira, P.J. Dijkstra, M. Karperien, C.A. van Blitterswijk, Z.Y. Zhong, J. Feijen, Injectable chitosan-based hydrogels for cartilage tissue engineering, Biomaterials 30 (2009) 2544–2551.
[14] R. Logithkumar, A. Keshavnarayan, S. Dhivya, A. Chawla, S. Saravanan, N. Selvamurugan, A review of chitosan and its derivatives in bone tissue engineering, Carbohydr. Polym. 151 (2016) 172–188.
[15] S. Saravanan, R.S. Leena, N. Selvamurugan, Chitosan based biocomposite scaffolds for bone tissue engineering, Int. J. Biol. Macromol. 93 (2016) 1354–1365.
[16] F. Croisier, C. Jerome, Chitosan-based biomaterials for tissue engineering, Eur. Polym. J. 49 (2013) 780–792.
[17] T. Jiang, M. Deng, R. James, L.S. Nair, C.T. Laurencin, Micro- and nanofabrication of chitosan structures for regenerative engineering, Acta Biomater. 10 (2014) 1632–1645.
[18] M.-H. Ho, P.-Y. Kuo, H.-J. Hsieh, T.-Y. Hsien, L.-T. Hou, J.-Y. Lai, D.-M. Wang, Preparation of porous scaffolds by using freeze-extraction and freeze-gelation methods, Biomaterials 25 (2004) 129–138.
[19] M.J. Moura, H. Faneca, M.P. Lima, M.H. Gil, M.M. Figueiredo, In situ forming chitosan hydrogels prepared via ionic/covalent co-cross-linking, Biomacromolecules 12 (2011) 3275–3284.
[20] S. Kim, Z.K. Cui, J. Fan, A. Fartash, T.L. Aghaloo, M. Lee, Photocrosslinkable chitosan hydrogels functionalized with the RGD peptide and phosphoserine to enhance osteogenesis, J. Mater. Chem. B 4 (2016) 5289–5298.
[21] P. Yilgor, K. Tuzlakoglu, R.L. Reis, N. Hasirci, V. Hasirci, Incorporation of a sequential BMP-2/BMP-7 delivery system into chitosan-based scaffolds for bone tissue engineering, Biomaterials 30 (2009) 3551–3559.
[22] S.V. Gohil, A. Padmanabhan, J. Deschamps, L.S. Nair, Chitosan-based scaffolds for growth factor delivery, in: J.D. Bumgardner (Ed.), Chitosan Based Biomaterials, vol. 2, Woodhead Publishing, 2017, pp. 175–207.
[23] Y.-P. Yun, S.E. Kim, E.Y. Kang, H.-J. Kim, K. Park, H.-R. Song, The effect of bone morphogenic protein-2 (BMP-2)-immobilizing heparinized-chitosan scaffolds for enhanced osteoblast activity, J. Tissue Eng. Regen. Med. 10 (2013) 122–130.
[24] R.S. T, M. G, Evaluation of RGD- or EGF-immobilized chitosan scaffolds for chondrogenic activity, Int. J. Biol. Macromol. 43 (2008) 121–128.
[25] S.K. Nandi, B. Kundu, D. Basu, Protein growth factors loaded highly porous chitosan scaffold: a comparison of bone healing properties, Mater. Sci. Eng. C 33 (2013) 1267–1275.
[26] A.H. Amir, A. Ghaee, Preparation of aminated chitosan/alginate scaffold containing halloysite nanotubes with improved cell attachment, Carbohydr. Polym. 151 (2016) 1120–1131.
[27] F.L. Mi, S.S. Shyu, S.T. Lee, T.B. Wong, Kinetic study of chitosan-tripolyphosphate complex reaction and acid-resistive properties of the chitosan-tripolyphosphate gel beads prepared by in-liquid curing method, J. Polym. Sci. B Polym. Phys. 37 (2015) 1551–1564.
[28] J.P. Gong, Y. Katsuyama, T. Kurokawa, Y. Osada, Double-network hydrogels with extremely high mechanical strength, Adv. Mater. 15 (2003) 1155–1158.
[29] S.L. Levengood, M. Zhang, Chitosan-based scaffolds for bone tissue engineering, J. Mater. Chem. B 2 (2014) 3161–3184.
[30] Y. Xu, J. Han, H. Lin, Fabrication and characterization of a self-crosslinking chitosan hydrogel under mild conditions without the use of strong bases, Carbohydr. Polym. 156 (2017) 372–379.
[31] F.L. Mi, H.W. Sung, S.S. Shyu, C.C. Su, C.K. Peng, Synthesis and characterization of biodegradable TPP/genipin co-crosslinked chitosan gel beads, Polymer 44 (2003) 6521–6530.
[32] C.W. Chou, H.J. Harn, Y.C. Hseu, Y.C. Shih, T.H. Wu, The effect and characteristics on chitosan nanoparticles with different concentration of TPP, Adv. Mater. Res. 123–125 (2010) 242–245.
[33] Z.W. Jing, Y.Y. Jia, N. Wan, M. Luo, M.L. Huan, T.B. Kang, S.Y. Zhou, B.L. Zhang, Design and evaluation of novel pH-sensitive ureido-conjugated chitosan/TPP nanoparticles targeted to *Helicobacter pylori*, Biomaterials 84 (2016) 276–285.
[34] M.M. Leane, R. Nankervis, A. Smith, L. Illum, Use of the ninhydrin assay to measure the release of chitosan from oral solid dosage forms, Int. J. Pharm. 271 (2004) 241–249.
[35] A. Nawaz, T.W. Wong, Quantitative characterization of chitosan in the skin by Fourier-transform infrared spectroscopic imaging and ninhydrin assay: application in transdermal sciences, J. Microsc. 263 (2015) 34–42.
[36] M. Gierszewska-Druzyńska, J. Ostrowska-Czubenko, Influence of crosslinking process conditions on molecular and supermolecular structure of chitosan hydrogel membrane, Prog. Chem. Appl. Chitin Its Deriv. 16 (2011) 15–22.
[37] Y.K. Min, J. Lee, Chitosan fibrous 3D networks prepared by freeze drying, Carbohydr. Polym. 84 (2011) 1329–1336.
[38] P. Sacco, M. Borgogna, A. Travan, E. Marsich, S. Paoletti, F. Asaro, M. Grassi, I. Donati, Polysaccharide-based networks from homogeneous chitosan-tripolyphosphate hydrogels: synthesis and characterization, Biomacromolecules 15 (2014) 3396–3405.
[39] S. Ladet, L. David, A. Domard, Multi-membrane hydrogels, Nature 452 (2008) 76–79.
[40] G. Li, X. Zhao, W. Zhao, L. Zhang, C. Wang, M. Jiang, X. Gu, Y. Yang, Porous chitosan scaffolds with surface micropatterning and inner porosity and their effects on Schwann cells, Biomaterials 35 (2014) 8503–8513.
[41] L.F.A.A. Raj, R. Jonisha, B. Revathi, E. Jayalakshmy, Preparation and characterization of BSA and chitosan nanopartices for sustainable delivery system for quercetin, J. Appl. Pharm. Sci. 5 (2015) 1–5.
[42] S. Salgin, U. Salgın, S. Bahadır, Zeta potentials and isoelectric points of biomolecules: the effects of ion types and ionic strengths, Int. J. Electrochem. Sci. 7 (2013) 12404–12414.
[43] E.A. Vogler, Protein adsorption in three dimensions, Biomaterials 33 (2012) 1201–1237.
[44] Y. Fu, W.J. Kao, Drug release kinetics and transport mechanisms of non-degradable and degradable polymeric delivery systems, Expert Opin. Drug Deliv. 7 (2010) 429–444.